10

Symmetric Supercapacitor Assembly and analysis of electrochemical performance

10.1. Introduction

Symmetric supercapacitor devices have been assembled with the prepared carbon electrodes from *P. juliflora* biomass and Zinc cobaltite electrode materials and the corresponding results are discussed in this Chapter. List of the assembled symmetric supercapacitor devices are:

(i) S-Carbon /PVA-KOH/ S-Carbon

(ii) B-Carbon /PVA-KOH/ B-Carbon

(iii) PB-Carbon /PVA-KOH/ PB-Carbon

(iv) $ZnCo_2O_4$/PVA-KOH/$ZnCo_2O_4$

(v) Fe,Cr:$ZnCo_2O_4$/PVA-KOH/Fe,Cr:$ZnCo_2O_4$

(vi) Ni,Cr:$ZnCo_2O_4$/PVA-KOH/Ni,Cr:$ZnCo_2O_4$

Prior to the assembly, electrochemical characteristics of the prepared materials are analysed and discussed in the earlier Chapters. The electrochemical characteristics of full cell assemblies are discussed in this Chapter.

10.2. Symmetric supercapacitor configurations

10.2.1. Electrochemical analysis of constructed symmetric supercapacitors with prepared carbons

The symmetric supercapacitor devices of S-Carbon//S-Carbon, B-Carbon//B-Carbon and PB-Carbon//PB-Carbon are constructed and the electrochemical performance of the device is tested by cyclic voltammetry (CV) and Galvanostatic charge-discharge (GCD) analysis. Gel polymer electrolyte, PVA-KOH, is used as an electrolyte for all the symmetric devices. The CV analysis of S-Carbon /PVA-KOH/ S-Carbon, B-Carbon /PVA-KOH/ B-Carbon and PB-Carbon /PVA-KOH/ PB-Carbon, shown in Figure 78a, 78b and 78c and the corresponding operating windows of the devices are 0V-1.2V, 0V-1.6V and 0V-1.6V

respectively. The behaviour of quasi-rectangular shape observed in the above-mentioned devices indicate the dominating contribution of electric double layer and minimal contribution of the pseudo-capacitive behaviour. The presence of non-cationic elements in S-Carbon, B-Carbon and PB-Carbon and the diffusion caused in the pores are considered to be responsible for the pseudo-capacitive nature of the device which are discussed in Chapter 4, 5 and 6. When the scan rate increases, the CV curves maintain their shapes with increase in current value suggesting an excellent capacitive behaviour of the devices. It is in line with the findings of the electrochemical behaviour of the carbon observed in three electrode systems.

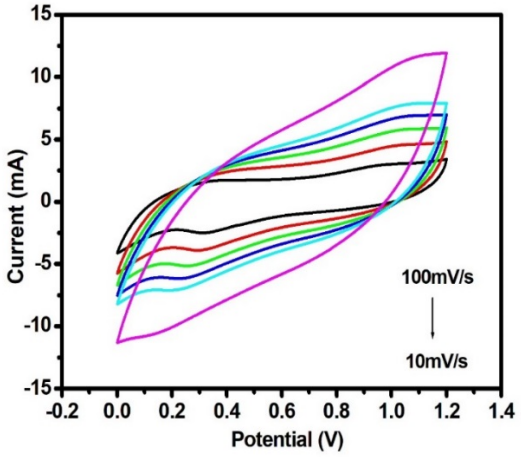

Figure 78a - Cyclic voltammogram of S-Carbon/PVA-KOH/S-Carbon

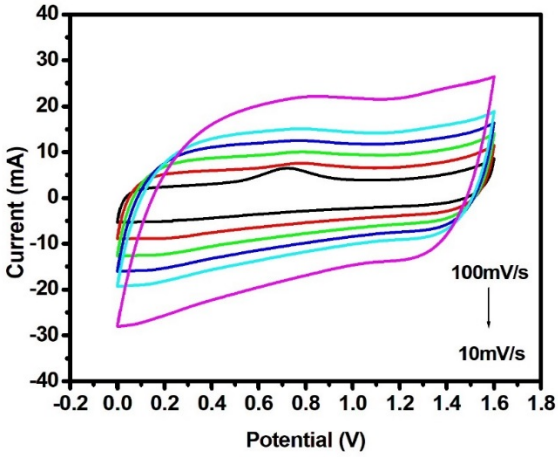

Figure 78b - Cyclic voltammogram of B-Carbon/PVA-KOH/B-Carbon

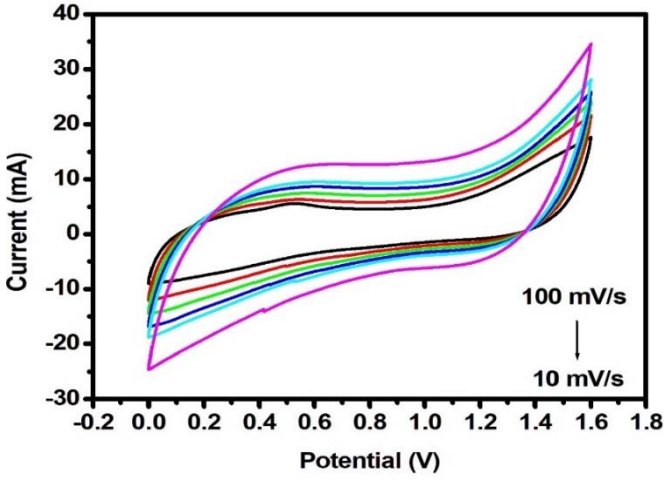

Figure 78c - Cyclic voltammogram of PB-Carbon/PVA-KOH/PB-Carbon

10.2.2. Kinetic analysis of the device using cyclic voltammograms

The quantitative estimation of charge storage mechanism can be found with kinetic analysis of CV recorded for the symmetric device fabricated, S-Carbon/PVA-KOH gel polymer electrolyte/S-Carbon. In this analysis capacitive and diffusive contributions are separated using the relationship between the current (i) and scan rate (v) given by Dunn power law:

$$i = av^{b} \quad (10)$$

where i is the current at specific voltage; v is the scan rate; a and b are constants. The total current given by the constructed device has contributions from (1) the capacitive-controlled process and (2) diffusion-controlled process. In equation (10), the value of b = 1 indicates capacitive-dominant behaviour, whereas b = 0.5 represents a diffusion-controlled process. Figure 79a, 79b and 79c shows the linear plot of assembled symmetric device with S-Carbon, B-Carbon and PB-Carbon. It gives the b value of 0.64, 0.77 and 0.72 for S-Carbon Vs S-Carbon, B-Carbon Vs B-Carbon and PB-Carbon Vs PB-Carbon respectively. It indicates that symmetric devices exhibit both capacitive and diffusion-controlled behaviour within the potential window of 0 to 1.2 V.

From CV analysis, the contribution of capacitive and diffusion-controlled charge-storage mechanisms are segregated by the following relation:

$$i(V) = K_1v + K_2v^{1/2} \quad (11)$$

where i(V) is the current response at a specific voltage; v is the scan rate; K_1v the capacitive current, and $K_2v^{1/2}$ is the diffusion-controlled current. The values of K_1 and K_2 are determined by measuring the current at various scan rates at particular voltage that can be used to separate the capacitive and diffusion-controlled processes.

Figure 80a, 80b and 80c shows the CV plot showing the segregated capacitive contribution (red region) to the total charge storage of the symmetric supercapacitor device, S-Carbon /PVA-KOH/ S-Carbon (48%), B-Carbon /PVA-KOH/ B-Carbon (72%), PB-Carbon /PVA-KOH/ PB-Carbon (57%) at 10 mV/s scan rate respectively. It indicates that the constructed B-Carbon Vs B-Carbon symmetric device has more capacitive dominance when compared to the other two symmetric devices. This may be correlated to the following facts: (i) higher atomic weight percentage of carbon, (ii) high surface area (iii) well-developed porous morphology (iv) low charge transfer resistance of B-Carbon in three electrode configurations as observed in half cell analysis and described in Chapter 5.

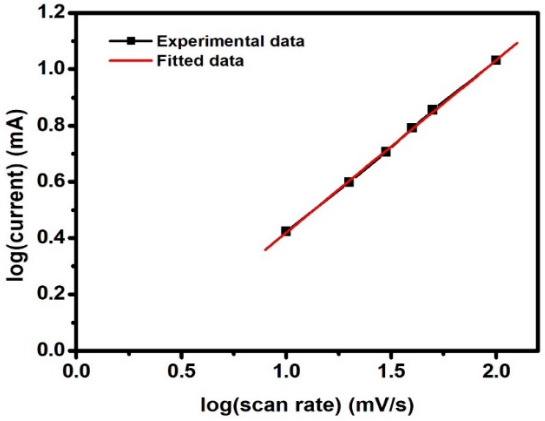

Figure 79a - Power law dependence of charge storage mechanism for S-Carbon/PVA-KOH/S-Carbon

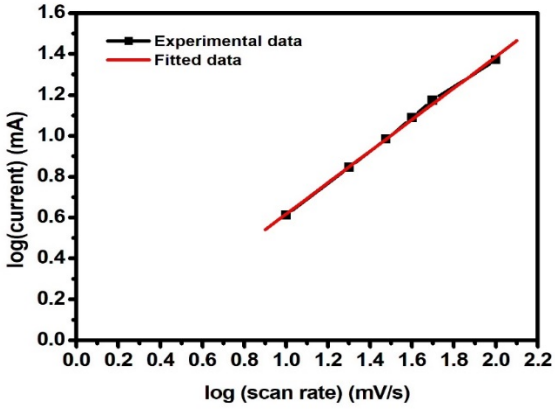

Figure 79b - Power law dependence of charge storage mechanism for B-Carbon/PVA-KOH/B-Carbon

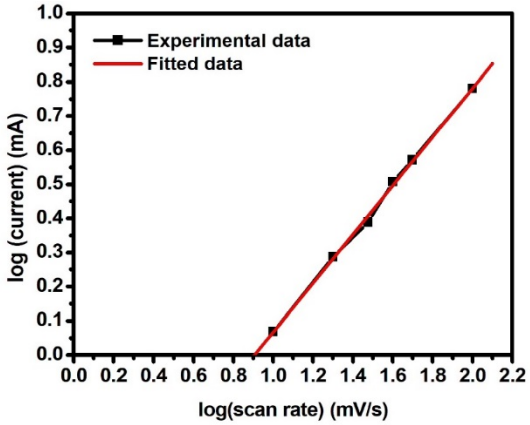

Figure 79c - Power law dependence of charge storage mechanism for PB-Carbon/PVA-KOH/PB-Carbon

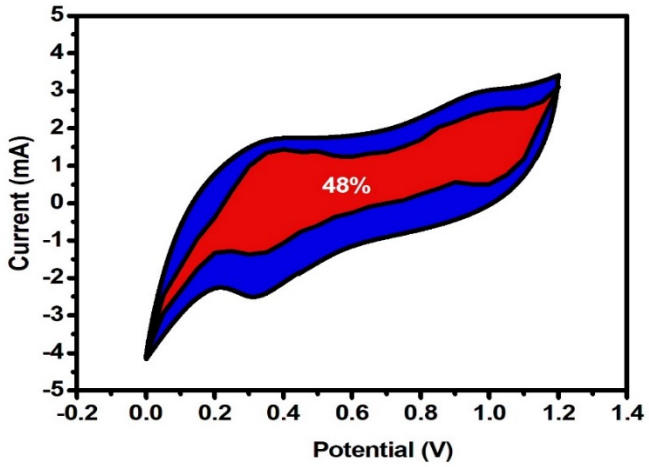

Figure 80a - Capacitive contribution of S-Carbon/PVA-KOH/S-Carbon device

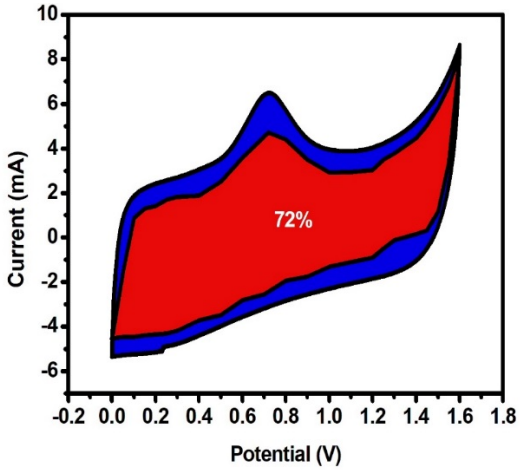

Figure 80b - Capacitive contribution of B-Carbon/PVA-KOH/B-Carbon device

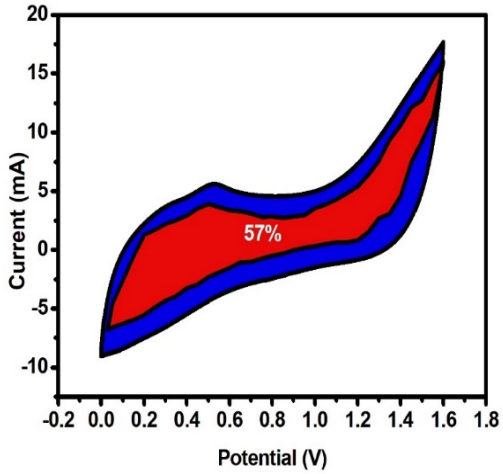

Figure 80c - Capacitive contribution of PB-Carbon/PVA-KOH/ PB-Carbon device

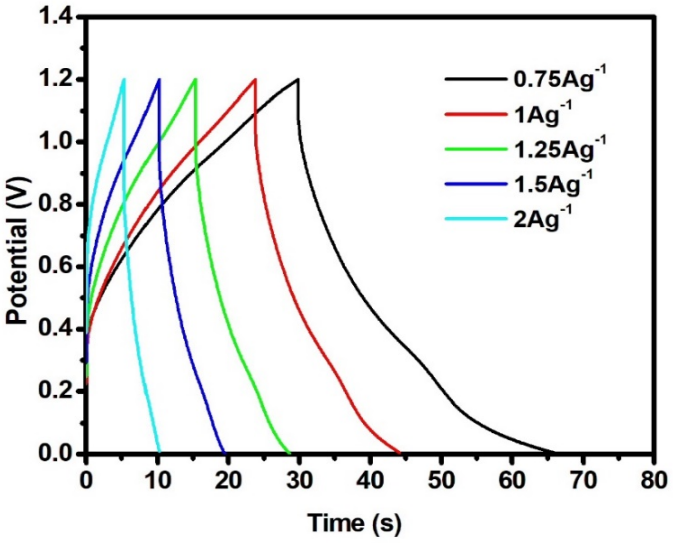

Figure 81a - Galvanostatic Charge-Discharge curves of S-Carbon/PVA-KOH/ S-Carbon device

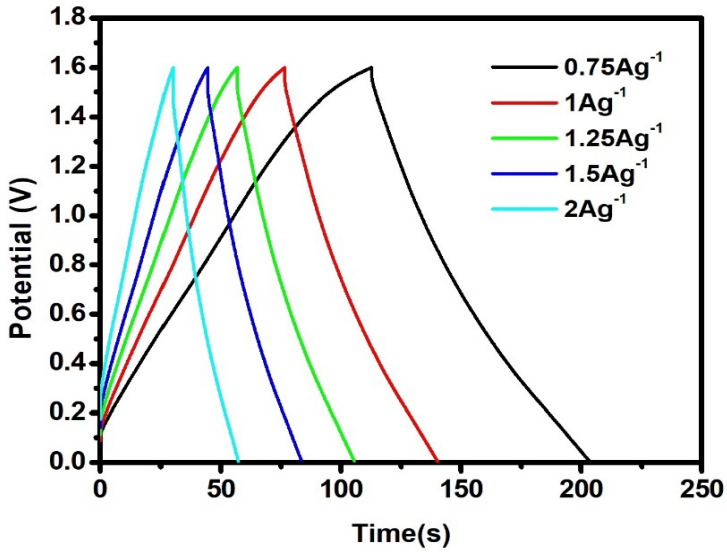

Figure 81b - Galvanostatic Charge-Discharge curves of B-Carbon/PVA-KOH/ B-Carbon device

In addition, GCD analysis has been carried out to investigate the capacitive behaviour of assembled symmetric device with the configuration of S-Carbon//S-Carbon, B-Carbon//B-Carbon and PB-Carbon//PB-Carbon respectively. The corresponding GCD curves for different current densities are shown in Figure 81a, 81b and 81c. The deviated triangular shape of the GCD curves suggests that the devices have both EDLC and

pseudocapacitive behaviours. In the S-Carbon//S-Carbon and PB-Carbon//PB-Carbon, the GCD curves are not symmetrical which leads to decrease in the performance of the device. Whereas, in the case of B-Carbon//B-Carbon charging and discharging time is more identical than S-Carbon vs S-Carbon , PB-Carbon vs PB-Carbon i.e., the discharge curves appear to be substantially symmetrical to the equivalent charge curves, implying that the B-Carbon/PVA-KOH/B-Carbon has outstanding capacitive performance than the other two devices that vouches the cyclic voltammogram results.

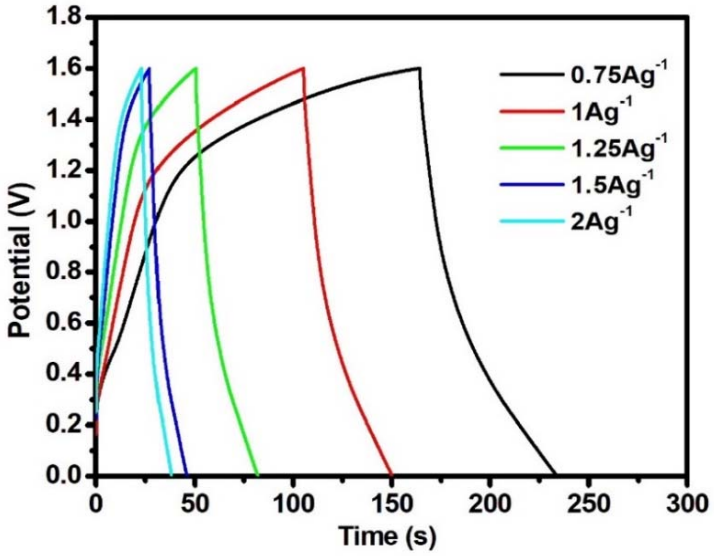

Figure 81c - Galvanostatic Charge-Discharge curves of PB-Carbon/PVA-KOH/ PB-Carbon device

The specific capacitance, energy and power density of S-Carbon /PVA-KOH/ S-Carbon, B-Carbon /PVA-KOH/ B-Carbon and PB-Carbon /PVA-KOH/ PB-Carbon symmetric supercapacitor devices are calculated from the GCD curves are shown in Table 34. The specific capacitances of all the fabricated two electrode devices lower than the specific capacitance of the half cells with S-Carbon, B-Carbon and PB-Carbon analysed in Chapter 4,5 and 6. Compared to solid electrolyte the rate of ion diffusion is high in aqueous electrolyte due to the higher fluidity and inter-particle space availability in the liquids. In the present case, device has been fabricated with solid electrolyte (PVA-KOH) and thus the ion diffusion rate is low which ultimately decreases the specific capacitance of the fabricated symmetric device with the configuration.

Compared to S-Carbon /PVA-KOH/ S-Carbon and PB-Carbon /PVA-KOH/ PB-Carbon, B-Carbon /PVA-KOH/ B-Carbon exhibits higher specific capacitance of 42.66 Fg^{-1} at a current density of 0.75 Ag^{-1}. In general, the energy storage mechanism of the constructed symmetric device is contributed from an electric double layer formed between electrode and the PVA-KOH electrolyte, which serves as the dielectric. When the charging voltage is applied, ions from the electrolyte are attracted to the electrode and the EDLC is formed. On the other hand, during the discharging process, the ions travel away from the electric double layer. As a result, the capacitance of an EDLC is proportional to the surface area of the electrode material. Due to the higher specific surface area of B-Carbon (explained in Chapter 4), the device assembled with B-Carbon has the higher specific capacitance than S-Carbon and PB-Carbon.

Table 34 - Gravimetric and areal performance of symmetric supercapacitor devices with carbon electrodes

Device	Current density ($A\ g^{-1}$)	Specific capacitance ($F\ g^{-1}$)	Specific energy density $WhKg^{-1}$	Specific power density (WKg^{-1})	Areal capacitance ($mF\ cm^{-2}$)	Areal energy density $\mu Wh/cm^2$	Areal power density $\mu W/cm^2$
S-Carbon /PVA-KOH/ S-Carbon	0.75	23.13	4.63	450	109.89	21.97	2138.40
	1	16.67	3.33	600	79.20	15.84	2851.20
	1.25	12.5	2.50	750	59.40	11.88	3564.00
	1.5	11.25	2.25	900	53.46	10.69	4276.80
	2	8.33	1.67	1200	39.60	7.92	5702.40
B-Carbon /PVA-KOH/ B-Carbon	0.75	42.66	15.17	600	387.66	137.83	5452.80
	1	40	14.22	800	363.52	129.25	7270.40
	1.25	38.28	13.61	1000	347.90	123.69	9088.00
	1.5	36.56	13.00	1200	332.28	118.14	10905.60
	2	33.63	11.95	1600	305.58	108.65	14540.80
PB-Carbon /PVA-KOH/ PB Carbon	**0.75**	30.47	10.83	600	292.50	104.00	5760
	1	26.25	9.33	800	252.00	89.60	7680
	1.25	24.22	8.61	1000	232.50	82.66	9600
	1.5	21.56	7.67	1200	207.00	73.60	11520
	2	20	7.11	1600	192.00	68.26	15360

The higher potential window of the B-Carbon device offers a maximum energy density of 14.22 Wh Kg^{-1} and a power density of 800 W Kg^{-1} at 1 Ag^{-1}. As expected from the excellent electrochemical performance of the half cell of B-carbon sample in standard three electrode configuration in Chapter 5 superior performance has been realized with the fabricated device. Also, the performance of the device with B-carbon in symmetric mode is found to be higher or comparable with already reported supercapacitor devices in symmetric mode listed in Table 35.

Table 35 - Comparison of Energy and Power density of fabricated symmetric device using prepared carbon with various literature

Material	Configuration	Energy density $WhKg^{-1}$	Power density WKg^{-1}	References
Mixture of *Birch, Fagaceae* and *Carpinus bitulus* - native European deciduous trees	Symmetric	0.53@ 2.5 Ag^{-1}	51	**Jain et al., (2021)**
Wood of *P. juliflora*	Symmetric	56.73@ 0.5 Ag^{-1}	249	**Selvaraj et al., (2021)**
houttuynia biomass	Symmetric	15.99@ 1 Ag^{-1}	500	**Shang et al., (2020)**
Squeezed *camellia oleifera* residue	Symmetric	9.55@ 0.5 Ag^{-1}	478	**Bo et al., (2019)**
Pods of *P. juliflora*	Symmetric	35.7@ 0.6 Ag^{-1}	971	**Shanmugapriya et al., (2019)**
Konjaku Flour	Symmetric	9.2@ 0.5 Ag^{-1}	250	**Lin et al., (2018)**
Natural casings	Symmetric	11.6@ 0.3 Ag^{-1}	297	**Xu et al., (2018)**
Pomelo peel	Symmetric	11.7@ 0.2 Ag^{-1}	160	**Wang et al., (2018)**
Poplar catkins	Symmetric	20.86	180.13	**Su et al., (2017)**
willow catkins	Symmetric	8.8	50	**Wang et al., (2017)**
Cotton stalk	Symmetric	18.14@0.5 Ag^{-1}	450.37	**Tian et al., (2017)**
Wood of *P. juliflora*	Symmetric	50@ 1 Ag^{-1}	150	**Sennu et al., (2016)**
Stick of *P. juliflora*	Symmetric	3.3@ 1 Ag^{-1}	600	**Present work**
Bark of *P.juliflora*	Symmetric	14.2@ 1 Ag^{-1}	800	**Present work**
Stick of *P. juliflora* by plasma firing	Symmetric	9.33@ 1 Ag^{-1}	800	**Present work**

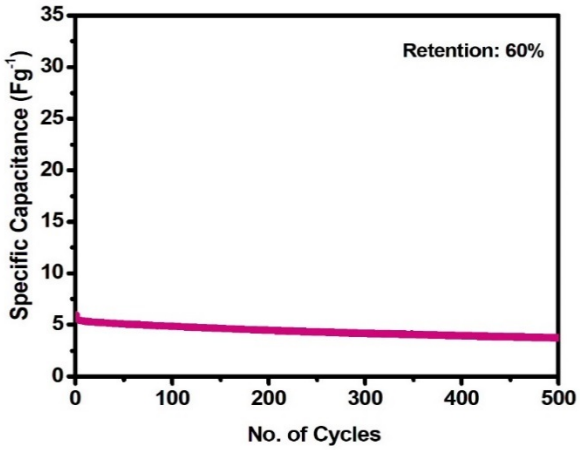

Figure 82a - Cyclic stability of S-Carbon /PVA-KOH/ S-Carbon device at 3 Ag^{-1}

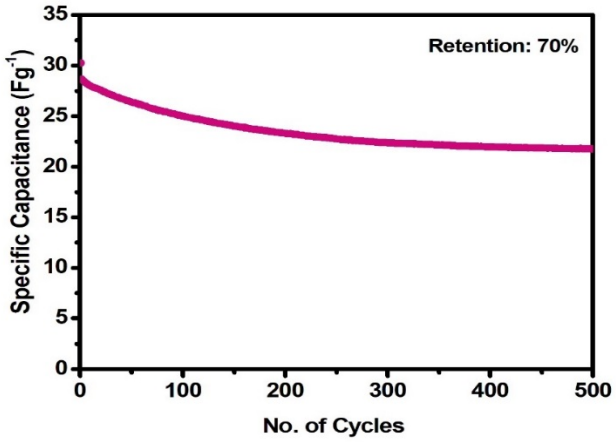

Figure 82b - Cyclic stability of B-Carbon /PVA-KOH/B-Carbon device at 3 Ag^{-1}

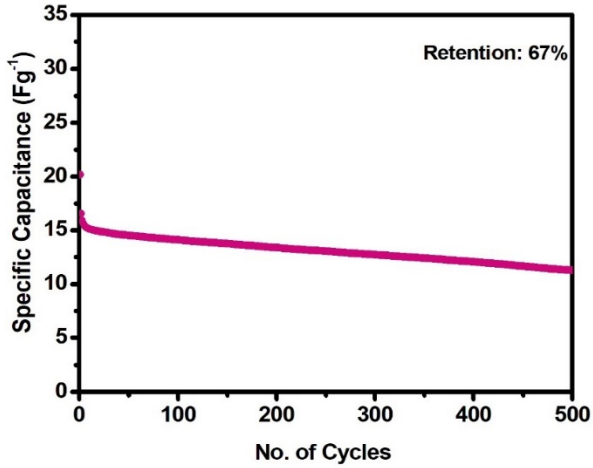

Figure 82c - Cyclic stability of PB-Carbon /PVA-KOH/PB-Carbon device at 3 Ag^{-1}

Testing the cyclic stability of the fabricated symmetric device with the configuration of S-Carbon /PVA-KOH/ S-Carbon and PB-Carbon /PVA-KOH/ PB-Carbon, B-Carbon /PVA-KOH/ B-Carbon over 500 cycles at 3 Ag^{-1}, the results are given in Figure 82a, 82b and 82c which shows 60%, 70% and 67% of capacity retention for S-Carbon//S-Carbon, B-Carbon// B-Carbon and PB-Carbon//PB-carbon respectively. The obtained value of 70% for B-Carbon// B-Carbon is higher than the symmetric devices assembled with S-Carbon and PB-Carbon indicating better cyclic stability of the electrochemical system with B-Carbon. It indicates that the PVA-KOH electrolyte is more suitable for B-Carbon than S-Carbon and PB-Carbon in symmetric device mode. In the case of symmetric device fabricated with B-Carbon, after 300 cycles, specific capacitance has maintained more or less constant whereas in the case of S-carbon and PB-Carbon symmetric devices, the specific capacitance has been continuously deteriorating even upto 500 cycles.

Electrochemical impedance spectroscopy (EIS) has been carried out to get a clear picture of capacitive behaviour in constructed S-Carbon /PVA-KOH/ S-Carbon, B-Carbon /PVA-KOH/ B-Carbon and PB-Carbon /PVA-KOH/ PB-Carbon devices which are shown in Figure 83a, 83b and 83c. The inset image of Figure 83a, 83b and 83c represents the equivalent circuit of the assembled devices. Corresponding fitted parameters of the device, before and after cycling are shown in Table 36, 37 and 38. Generally, compared with three electrode configuration of S-Carbon, B-Carbon and PB-Carbon, internal resistance of device in two electrode electrochemical system is high. In contrast to three electrode configuration, undesired resistive factors due to the dielectric changes brought by the polymeric electrolyte has resulted in a significantly larger internal resistance.

The Nyquist plot shows the semicircle in high frequency region which relates to the charge transfer resistance. After cycling, the internal resistance (R_s) of S-Carbon// S-Carbon B-Carbon//B-Carbon and PB-Carbon// PB-Carbon increases due to the formation SEI layer. But in the case of, B-Carbon Vs B-Carbon, Warburg resistance is decreased due to effective contact between the PVA-KOH electrolyte separator and B-Carbon electrodes. Apart from the resistive components, two constant phase elements (CPE) have been observed in the present case. The CPE emerges from the diffusion of electrolytic ions into the pores of the electrode and inhomogeneity at the electrode/electrolyte interface **(Rafik et al., 2007)**. In the symmetric devices, the CPE existence and the change in CPE

values with cycling may be ascribed to the distribution of active sites across the carbon electrode. After cycling, both n1 and n2 values (n <0.5) obtained out of fitting which indicates the dominance of capacitive behaviour in B-Carbon//B-Carbon device. Hence, the cyclic performance of the device has been improved. In other two cases, n2 value goes down towards 0.5 suggesting that diffusive behaviour of the device. Hence, the cyclic stability of the S-Carbon//S-Carbon and PB-Carbon//PB-Carbon is lower than the device fabricated with B-Carbon.

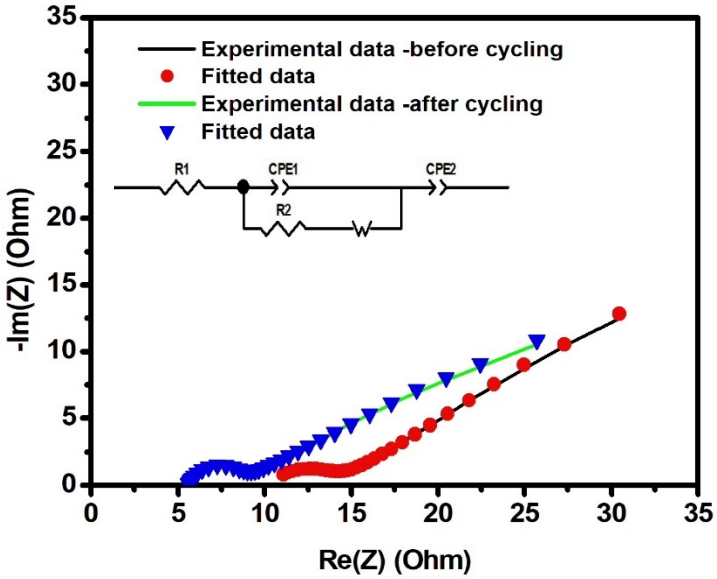

Figure 83a - Electrochemical impedance spectra of S-Carbon /PVA-KOH/S-Carbon device

Table 36 - Fitted parameters of electrochemical impedance spectra of S-Carbon /PVA-KOH/ S-Carbon device

Parameters	Before Cycling	After Cycling
$R_1(\Omega)$	10.25	5.47
$R_2(\Omega)$	3.66	2.55
CPE 1	0.52×10^{-3}	0.06×10^{-3}
n1	0.66	0.95
CPE 2	0.15	0.07
n2	0.3	0.34
W	2.51	7.15

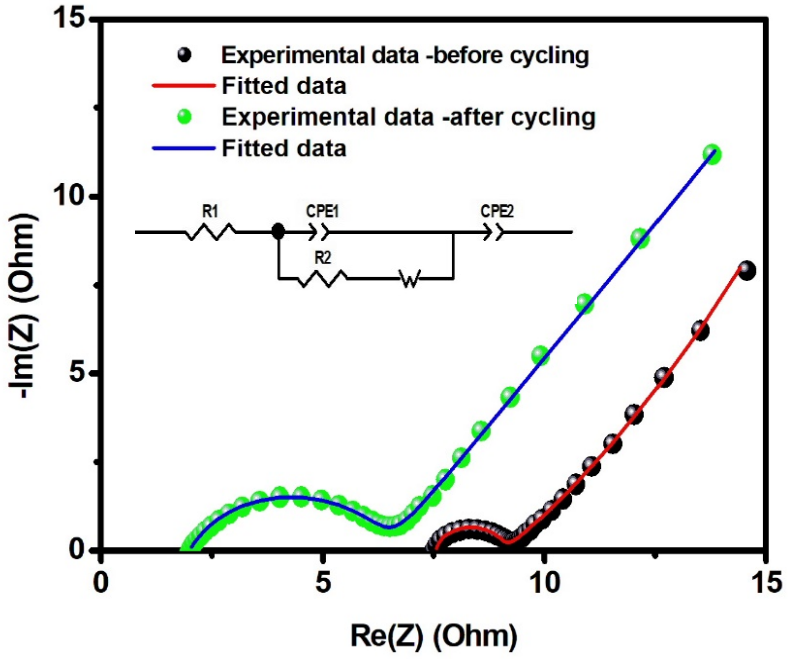

Figure 83b - Electrochemical impedance spectra of B-Carbon /PVA-KOH/ B-Carbon device

Table 37 - Fitted parameters of electrochemical impedance spectra of B-Carbon/PVA-KOH/ B-Carbon device

Parameters	Before Cycling	After Cycling
$R_1(\Omega)$	7.54	1.98
$R_2(\Omega)$	1.53	4.44
CPE 1	0.07×10^{-3}	0.40×10^{-3}
n1	0.89	0.75
CPE 2	0.59	0.11
n2	0.99	0.64
W	4.22	0.71

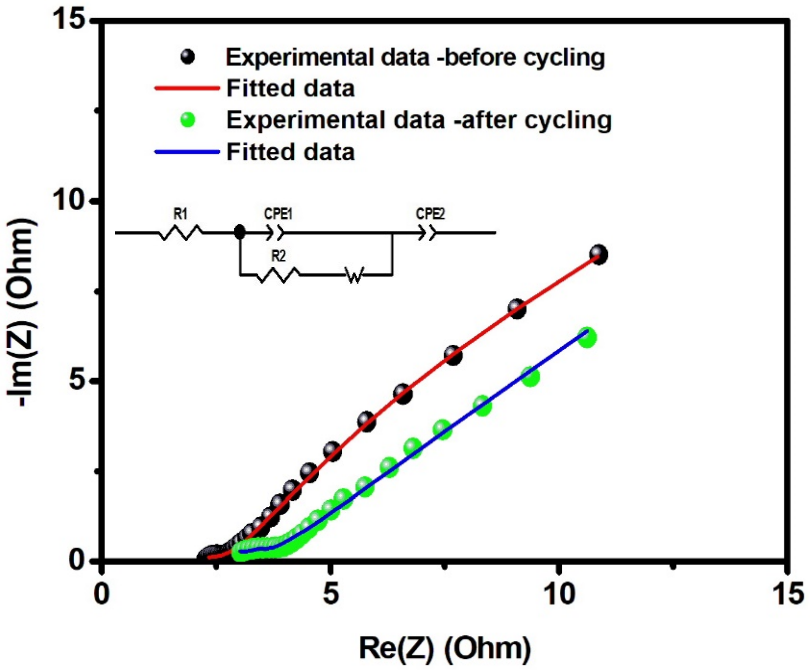

Figure 83c - Electrochemical impedance spectra of PB-Carbon /PVA-KOH/ PB-Carbon device

Table 38 - Fitted parameters of electrochemical impedance spectra of PB-Carbon /PVA-KOH/ PB-Carbon device

Parameters	Before Cycling	After Cycling
$R_1(\Omega)$	1.42	1.51
$R_2(\Omega)$	3.28	2.393
CPE 1	0.09	$9.23x10^{-3}$
n1	0.67	0.29
CPE 2	0.30	0.82
n2	0.3	0.34
W	5.06	12.44

10.3. Electrochemical analysis of constructed symmetric supercapacitor devices of undoped and doped $ZnCo_2O_4$

The electrochemical performance of the fabricated $ZnCo_2O_4$/PVA-KOH/$ZnCo_2O_4$, FeCr:$ZnCo_2O_4$/PVA-KOH/Fe,Cr:$ZnCo_2O_4$ and Ni,Cr:$ZnCo_2O_4$/PVA-KOH/Ni,Cr:$ZnCo_2O_4$ symmetric full cell devices are tested in two-electrode configuration. The working window of the device of the devices are 0V- 1 V, 0V-1V and 0V -1.2 V respectively, which are shown in Figure 84a, 84b and 84c. It shows distorted rectangular profile with minimal faradic reactions at each scan rate which emerges from the combination of electric double layer and pseudocapacitive mechanisms. From the linear relationship between scan rate and current at a specific voltage, Figure 85a, 85b and 85c, the kinetics of the charge-storage of assembled devices can be described. The calculated slope (b) value for $ZnCo_2O_4$//$ZnCo_2O_4$, FeCr:$ZnCo_2O_4$//Fe,Cr:$ZnCo_2O_4$ and Ni,Cr:$ZnCo_2O_4$//Ni,Cr:$ZnCo_2O_4$ fabricated symmetric devices are 0.60, 0.68 and 0.85 respectively, intimates the charge storage involving both diffusion controlled and capacitive controlled process. These can be separated using the equation (11).

The capacitive contribution separated from the total contribution of the CV curve at lower scan rate of 10 mV/s and are shown in Figure 86a, 86b and 86c. It shows the trend of both diffusive and capacitive controlled process. The contribution of 54%, 57% and 48% of the capacitive controlled process are observed for $ZnCo_2O_4$//$ZnCo_2O_4$, FeCr:$ZnCo_2O_4$//Fe,Cr:$ZnCo_2O_4$ and Ni,Cr:$ZnCo_2O_4$//Ni,Cr:$ZnCo_2O_4$ respectively. Comparatively, the value of Ni and Cr doped Zinc cobaltite is lower than the device assembled with pure and Fe, Cr doped Zinc cobaltite. It is due to the addition of Ni and Cr dopants into the pristine material enhancing the redox behaviour than capacitive behaviour which is clearly seen from the shape of the CV curve of Ni,Cr:$ZnCo_2O_4$ /PVA-KOH/ Ni,Cr:$ZnCo_2O_4$. It shows noticeable faradaic behaviour than other two devices such as $ZnCo_2O_4$ /PVA-KOH/ $ZnCo_2O_4$ and Fe,Cr:$ZnCo_2O_4$ /PVA-KOH/ Fe,Cr:$ZnCo_2O_4$.

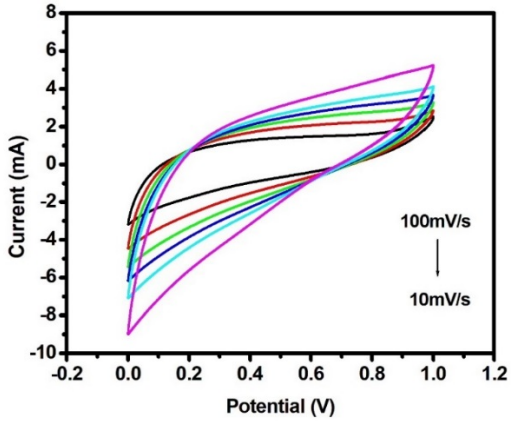

Figure 84a - Cyclic voltammogram of $ZnCo_2O_4$/PVA-KOH/$ZnCo_2O_4$ device

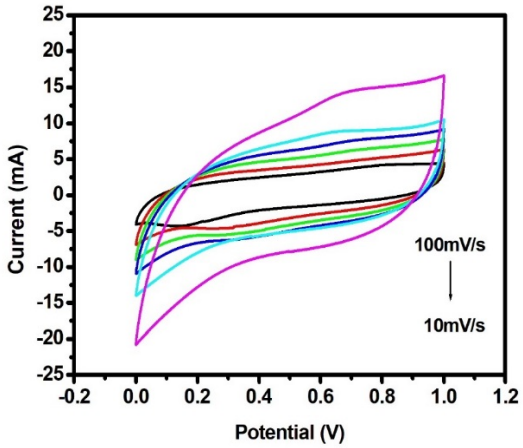

Figure 84b - Cyclic voltammogram of Fe,Cr:$ZnCo_2O_4$ /PVA-KOH/ Fe,Cr:$ZnCo_2O_4$ device

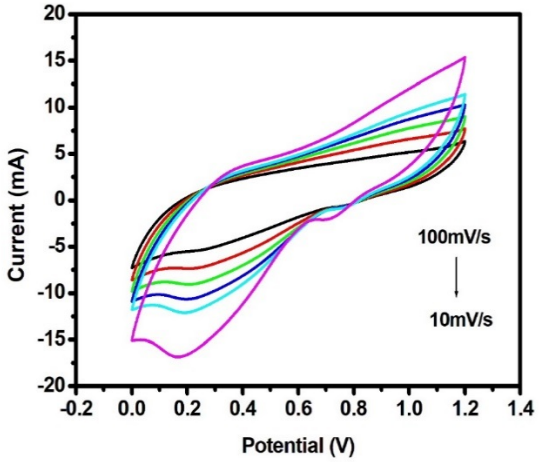

Figure 84c - Cyclic voltammogram of Ni,Cr:$ZnCo_2O_4$ /PVA-KOH/ Ni,Cr:$ZnCo_2O_4$ device

Figure 87a, 87b and 87c displays the GCD curves of $ZnCo_2O_4$/PVA-KOH/$ZnCo_2O_4$, Fe,Cr:$ZnCo_2O_4$/PVA-KOH/Fe,Cr:$ZnCo_2O_4$ and Ni,Cr:$ZnCo_2O_4$/PVA-KOH/Ni,Cr:$ZnCo_2O_4$, tested with various current densities. The obtained GCD curves are agrees with the results observed from the CV measurements. By using the relation (2), specific capacitance of the fabricated devices are calculated. The calculated parameters from the GCD analysis of fabricated devices are shown in Table 39. Compared to device assembled with undoped $ZnCo_2O_4$ material, the device assembled with Fe and Cr doped Zinc cobaltite shows the higher energy density of 4.16 Wh Kg^{-1} with a power density of 500 W Kg^{-1} at 1 Ag^{-1} which ensures the fact that the addition of dopants into pristine matrix enhances the electrochemical performance of the device. Also, the values of obtained specific energy and power density of Ni,Cr:$ZnCo_2O_4$/PVA-KOH/Ni,Cr:$ZnCo_2O_4$ is higher than the pure Zinc cobaltite. The results are compared with reported articles of Zinc cobaltite based symmetric supercapacitors **(Mary & Bose, 2018; Raut & Sankapal, 2017).** The similar devices constructed with by two authors are worth mentioning at this juncture. The first report is by Mary et al., with similar device with $ZnCo_2O_4$ prepared by hydrothermal method and KOH is impregnated in a non-woven cloth and the electrodes are coated on Ni foam. Energy density achieved is 0.49 Wh Kg^{-1} with a power density. The second setup is with $ZnCo_2O_4$ prepared on stainless steel plate using SILAR method as thin films and KOH is coated on either plates to attach them face to face forming the device. This has given an energy density of 9.67 Wh Kg^{-1} with power density of 1450 W Kg^{-1} at 1 Ag^{-1}. In the present case, the method of preparation and the selection of current collector is very less expensive which could give a power density upto 1200 W Kg^{-1}. However, the areal performance is higher for Ni,Cr:$ZnCo_2O_4$/PVA-KOH/Ni,Cr:$ZnCo_2O_4$ other than the two devices. The better areal performance of the Ni and Cr doped device offers more compatibility thus could accommodate space reduction in commercial applications.

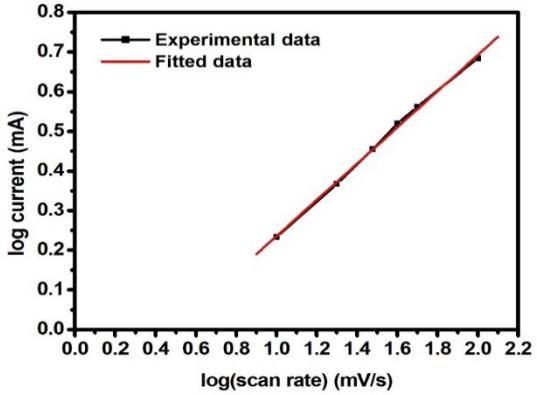

Figure 85a - Power law dependence of charge storage mechanism for $ZnCo_2O_4$/PVA-KOH/$ZnCo_2O_4$ device

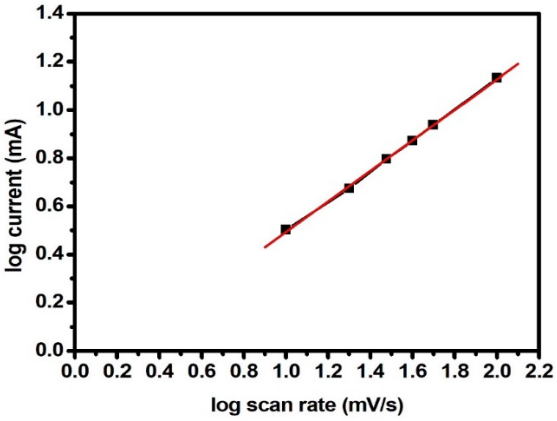

Figure 85b - Power law dependence of charge storage mechanism for Fe,Cr:$ZnCo_2O_4$ /PVA-KOH/ Fe,Cr:$ZnCo_2O_4$ device

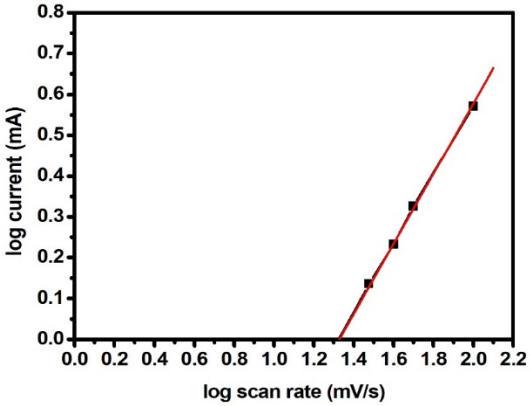

Figure 85c - Power law dependence of charge storage mechanism for Ni,Cr:$ZnCo_2O_4$ /PVA-KOH/ Ni,Cr:$ZnCo_2O_4$ device

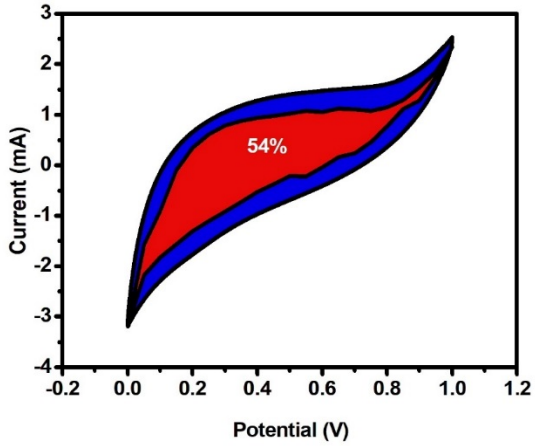

Figure 86a - Capacitive contribution of $ZnCo_2O_4$/PVA-KOH/$ZnCo_2O_4$ device

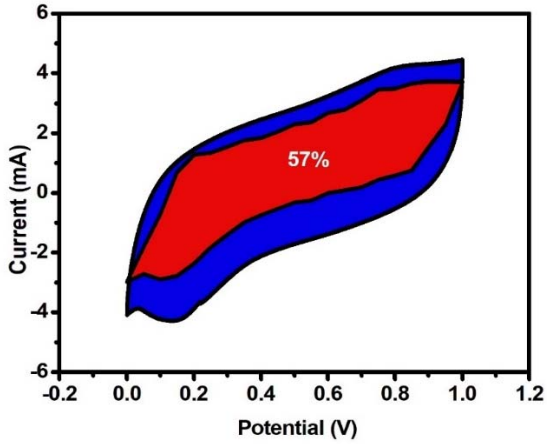

Figure 86b - Capacitive contribution of Fe,Cr:$ZnCo_2O_4$/PVA-KOH/ Fe,Cr:$ZnCo_2O_4$ device

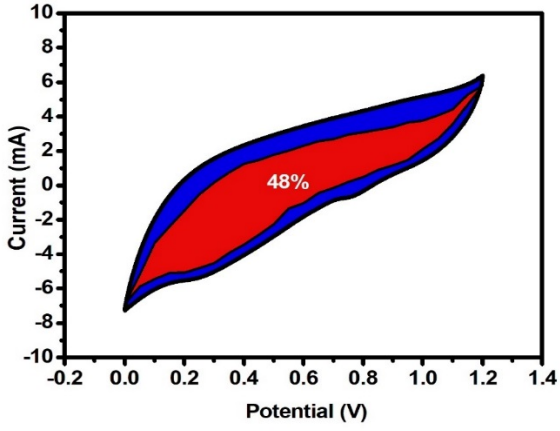

Figure 86c - Capacitive contribution of Ni,Cr:$ZnCo_2O_4$/PVA-KOH/ Ni,Cr:$ZnCo_2O_4$ device

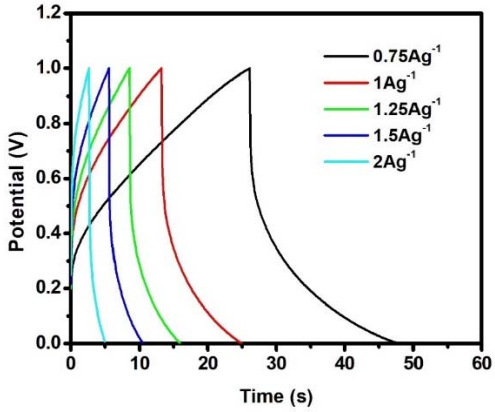

Figure 87a - Galvanostatic Charge-Discharge curves of $ZnCo_2O_4$/PVA-KOH/$ZnCo_2O_4$ device

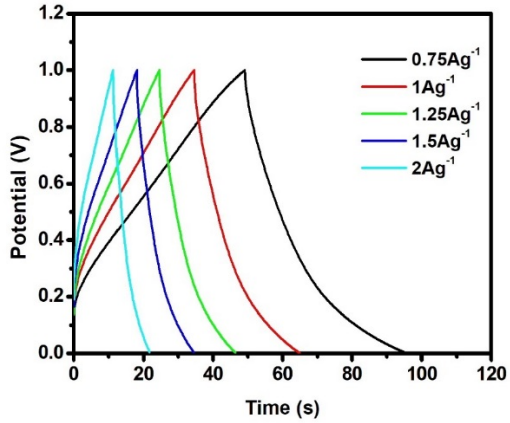

Figure 87b - Galvanostatic Charge-Discharge curves of Fe,Cr:$ZnCo_2O_4$ /PVA-KOH/ Fe,Cr:$ZnCo_2O_4$ device

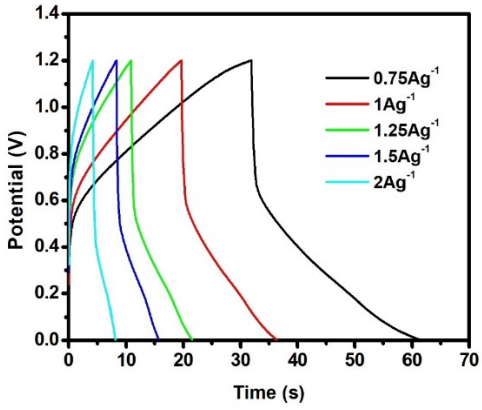

Figure 87c - Galvanostatic Charge-Discharge curves of Ni,Cr:$ZnCo_2O_4$/PVA-KOH/ Ni,Cr:$ZnCo_2O_4$ device

Table 39 - Gravimetric and areal performance of symmetric supercapacitor device with doped and undoped $ZnCo_2O_4$ electrodes

Device	Current density ($A\ g^{-1}$)	Specific capacitance ($F\ g^{-1}$)	Specific energy density $Wh\ Kg^{-1}$	Specific power density (WKg^{-1})	Areal capacitance ($mF\ cm^{-2}$)	Areal energy density $\mu Wh/cm^2$	Areal power density $\mu W/cm^2$
$ZnCo_2O_4$/PVA-KOH/$ZnCo_2O_4$	0.75	21	2.19	375	45.28	6.28	1078.12
	1	11.9	1.65	500	34.21	4.75	1437.50
	1.25	7.4	1.28	625	26.59	3.69	1796.87
	1.5	4.97	1.04	750	21.43	2.97	2156.25
	2	2.4	0.67	1000	13.80	1.91	2875.00
Fe,Cr: $ZnCo_2O_4$/PVA-KOH/ Fe,Cr:$ZnCo_2O_4$	0.75	48	5.00	375	115.2	16	1200
	1	30	4.16	500	96	13.33	1600
	1.25	22	3.82	625	88	12.22	2000
	1.5	17	3.54	750	81.6	11.33	2400
	2	11	3.05	1000	70.4	9.78	3200
Ni,Cr:$ZnCo_2O_4$/PVA-KOH/Ni,Cr:$ZnCo_2O_4$	**0.75**	18.75	3.75	450	91.80	18.36	2203.2
	1	14	2.8	600	68.544	13.70	2937.6
	1.25	11.25	2.25	750	55.08	11.01	3672.0
	1.5	9.38	1.86	900	45.90	9.18	4406.4
	2	6.33	1.27	1200	31.008	6.20	5875.2

The cyclic performance of $ZnCo_2O_4$/PVA-KOH/$ZnCo_2O_4$, FeCr:$ZnCo_2O_4$/PVA-KOH/Fe,Cr:$ZnCo_2O_4$ and Ni,Cr:$ZnCo_2O_4$/PVA-KOH/Ni,Cr:$ZnCo_2O_4$ symmetric supercapacitor has been carried out at a current density of 3 Ag^{-1} is given in Figure 88a, 88b and 88c. As seen from this figure, 53%, 68% and 63% of specific capacitance has been retained after 500 charge–discharge cycles for $ZnCo_2O_4$//$ZnCo_2O_4$, FeCr:$ZnCo_2O_4$//Fe,Cr:$ZnCo_2O_4$ and Ni,Cr:$ZnCo_2O_4$//Ni,Cr:$ZnCo_2O_4$ symmetric devices. Symmetric devices fabricated with doped Zinc cobaltite exhibits higher capacity retention over 500 cycles. It is due to the incorporation of dopants into the pristine material bringing in structural stability and higher cyclability.

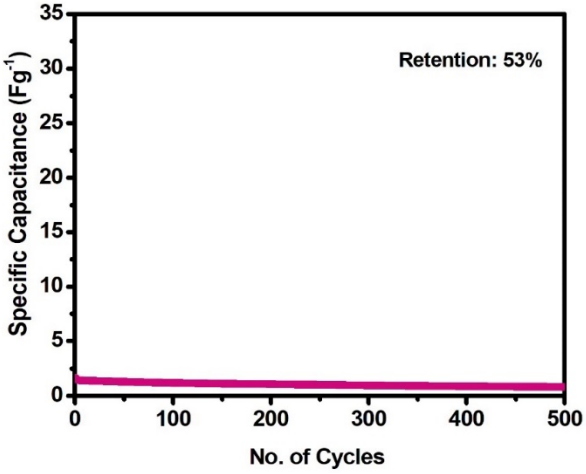

Figure 88a - Cyclic stability of $ZnCo_2O_4$/PVA-KOH/$ZnCo_2O_4$ device

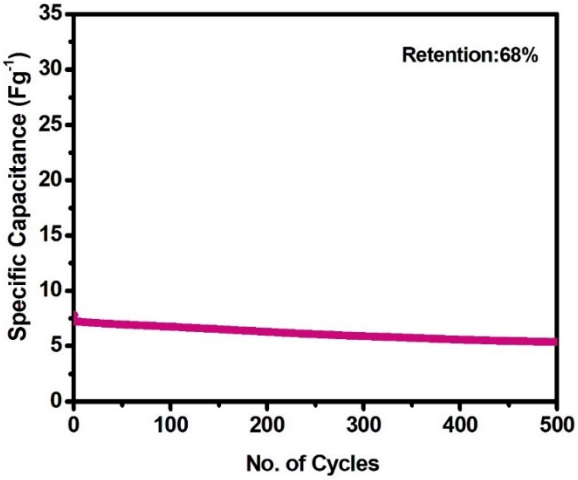

Figure 88b - Cyclic stability of Fe,Cr:$ZnCo_2O_4$ /PVA-KOH/ Fe,Cr:$ZnCo_2O_4$ device

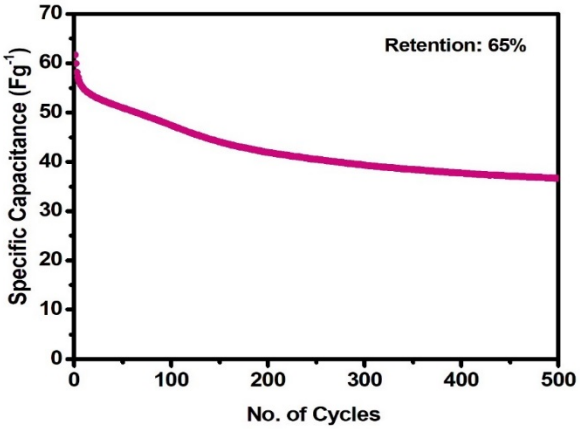

Figure 88c - Cyclic stability of Ni,Cr:$ZnCo_2O_4$ /PVA-KOH/ Ni,Cr:$ZnCo_2O_4$ device

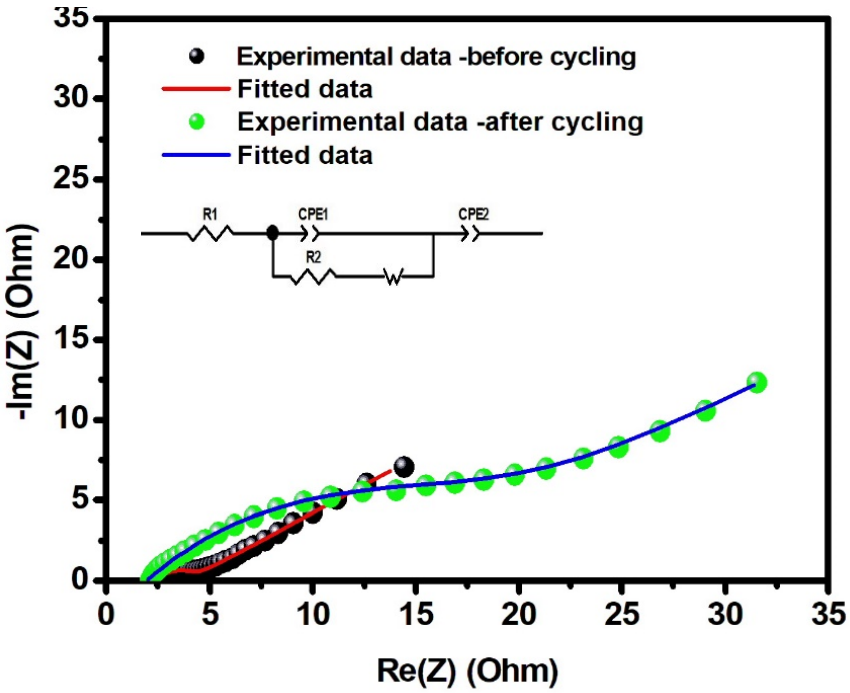

Figure 89a - Electrochemical impedance spectra of $ZnCo_2O_4$/PVA-KOH/$ZnCo_2O_4$ device

Table 40 - Fitted parameters of electrochemical impedance spectra of $ZnCo_2O_4$/PVA-KOH/$ZnCo_2O_4$ device

Parameters	Before Cycling	After Cycling
$R_1(\Omega)$	2.47	1.92
$R_2(\Omega)$	1.421	13.8
CPE 1	0.57×10^{-3}	5.90×10^{-3}
n1	0.76	0.60
CPE 2	0.10	0.06
n2	0.38	0.39
W	0.10	8.19

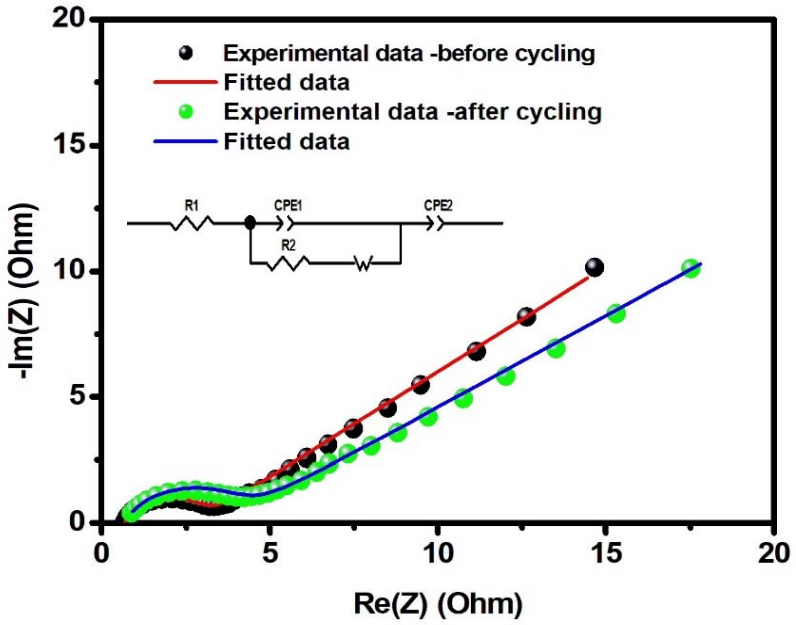

Figure 89b - Electrochemical impedance spectra of Fe,Cr:$ZnCo_2O_4$/PVA-KOH/ Fe,Cr:$ZnCo_2O_4$ device

Table 41 - Fitted parameters of electrochemical impedance spectra of Fe,Cr:$ZnCo_2O_4$ /PVA-KOH/ Fe,Cr:$ZnCo_2O_4$ device

Parameters	Before Cycling	After Cycling
$R_1(\Omega)$	0.56	0.61
$R_2(\Omega)$	1.90	3.09
CPE 1	0.10×10^{-3}	0.35×10^{-3}
n1	0.93	0.79
CPE 2	0.40	0.06
n2	0.20	0.40
W	6.85	1.42

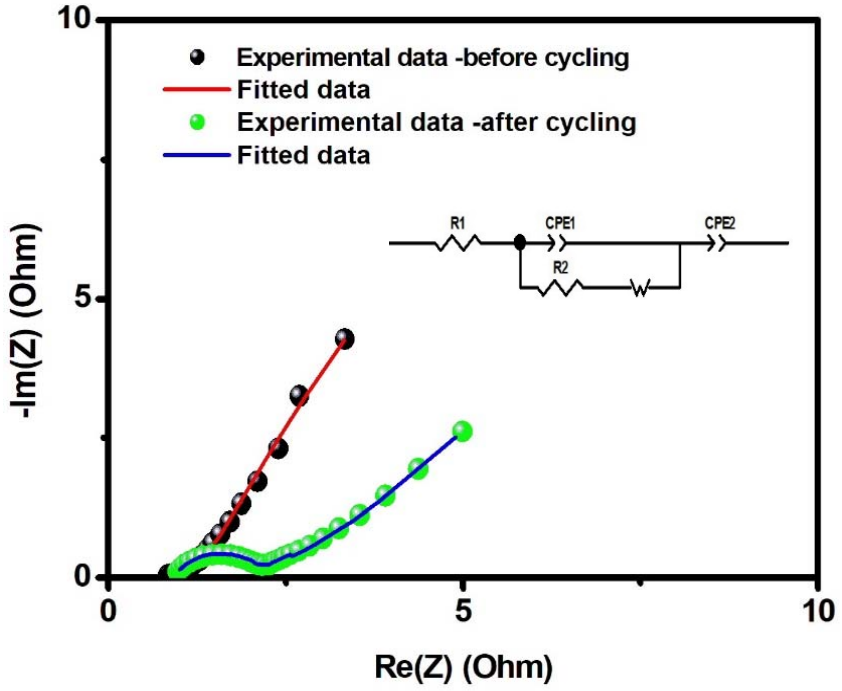

Figure 89c - Electrochemical impedance spectra of Ni,Cr:$ZnCo_2O_4$/PVA-KOH/ Ni,Cr:$ZnCo_2O_4$ device

Table 42 - Fitted parameters of electrochemical impedance spectra of Ni,Cr:$ZnCo_2O_4$/PVA-KOH/Ni,Cr:$ZnCo_2O_4$ device

Parameters	Before Cycling	After Cycling
$R_1(\Omega)$	0.92	0.79
$R_2(\Omega)$	1.13	3.28
CPE 1	1.20×10^{-3}	0.34
n1	0.77	0.84
CPE 2	0.58	0.98
n2	0.43	0.21
W	1.01	1.28

Impedance spectra of $ZnCo_2O_4$ /PVA-KOH/ $ZnCo_2O_4$, Fe, Cr: $ZnCo_2O_4$ /PVA-KOH/ Fe,Cr:$ZnCo_2O_4$ and Ni, Cr: $ZnCo_2O_4$ /PVA-KOH/ Ni,Cr:$ZnCo_2O_4$ has been evaluated in the frequency range of 100 mHz to10 KHz given in Figure 89a, 89b and 89c. The fitted equivalent circuit is shown in the inset. The fitted parameters with EC lab software of electrochemical impedance analysis are shown in Table 40, 41 and 42. After cycling, the internal resistance has increased for all the three symmetric devices which is similar to the observations seen in the previous devices. However, after cycling, the charge transfer resistance of Fe,Cr: $ZnCo_2O_4$ /PVA-KOH/ Fe,Cr:$ZnCo_2O_4$ is low compared to the device assembled with $ZnCo_2O_4$ /PVA-KOH/ $ZnCo_2O_4$ and Ni, Cr: $ZnCo_2O_4$ /PVA-KOH/ Ni,Cr:$ZnCo_2O_4$. This fact increases the electrochemical stability of the Fe, Cr doped zinc cobaltite based device over 500 cycles to 68% compared to 54% in pure $ZnCo_2O_4$ and 63% in Ni,Cr: $ZnCo_2O_4$. The n1 value of Fe,Cr: $ZnCo_2O_4$ /PVA-KOH/ Fe,Cr:$ZnCo_2O_4$ is high, 0.79, along with the fact that the Warburg impedance which corresponds to the diffusive component has decreased. This may be corroborated with better performance in Fe,Cr:$ZnCo_2O_4$ symmetric device than other two devices. It is similar to the cyclic stability obtained in three electrode configuration of Fe, Cr: $ZnCo_2O_4$. Compared to Fe,Cr: $ZnCo_2O_4$ /PVA-KOH/ Fe,Cr:$ZnCo_2O_4$ and Ni,Cr: $ZnCo_2O_4$ /PVA-KOH/ Ni,Cr:$ZnCo_2O_4$, the Warburg resistance is high for $ZnCo_2O_4$ $ZnCo_2O_4$ which indicates the excellent capacitive behaviour of symmetric devices assembled with doped samples.

Summary

Among all the fabricated symmetric devices using carbon based electrodes, B-Carbon/PVA-KOH/B-Carbon symmetric device exhibits better electrochemical performance than other fabricated devices based on carbon electrodes due to its high capacitive contribution (72%).

Figure 90 shows the comparison of Ragone plot of all the fabricated symmetric supercapacitor devices drawn with the corresponding values of energy and power density of each device constructed. The better capacitive performance of B-Carbon in three electrode configuration and high specific surface area of B-Carbon gives rise to increase in the performance of the B-Carbon/PVA-KOH/B-Carbon symmetric device.

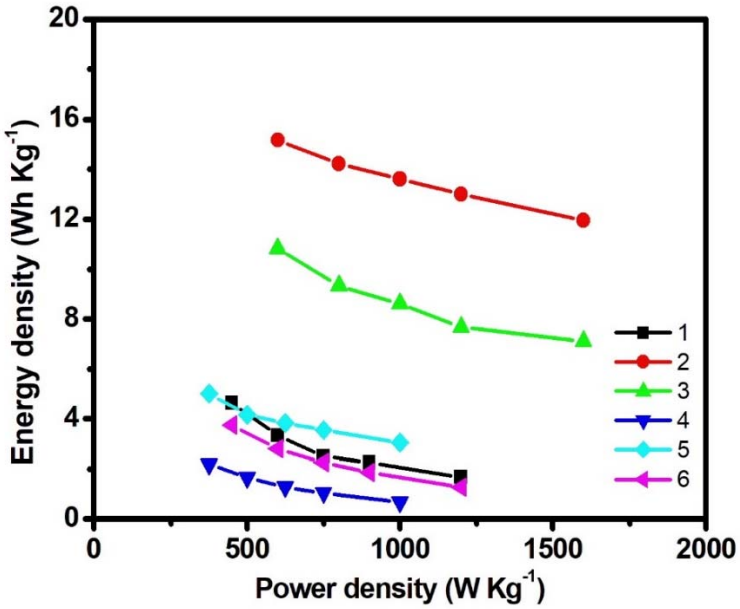

1.**S-Carbon /PVA-KOH/ S-Carbon**

2. B-Carbon /PVA-KOH/ B-Carbon

3.PB- carbon/PVA-KOH/PB-carbon

4.$ZnCo_2O_4$/PVA-KOH/ $ZnCo_2O_4$

5.Fe, Cr: $ZnCo_2O_4$/PVA-KOH/Fe, Cr: $ZnCo_2O_4$

6.Ni,Cr: $ZnCo_2O_4$/PVA-KOH/Ni,Cr:$ZnCo_2O_4$

Figure 90 - Comparison of Energy and Power density of all fabricated symmetric supercapacitor devices – Ragone plot

It exhibits higher energy density of 15.17 Wh Kg^{-1} and power density of 600 W Kg^{-1} at the current density of 0.75 Ag^{-1}. From all the symmetric devices assembled with metal oxides, Fe,Cr:$ZnCo_2O_4$/PVA-KOH/ Fe,Cr:$ZnCo_2O_4$ exhibits better gravimetric performance than other Zinc cobaltite based devices. However, the areal performance of the Ni,Cr:$ZnCo_2O_4$/PVA-KOH/ Ni,Cr:$ZnCo_2O_4$ shows higher value than other two symmetric devices assembled with $ZnCo_2O_4$ and Fe,Cr:$ZnCo_2O_4$. In nutshell, out of all the six different combination of symmetric devices, B-Carbon performs the best with 72% capacitive component with more cyclic stability of 70%.